DESIGN AND TECHNICAL VALIDATION OF INDUSTRIAL TRANSFORMER SUBSTATIONS WITH INTEGRATED ELECTRIC VEHICLE CHARGING INFRASTRUCTURE

Kaan Mehmet Toprak[1], Musa Terkeş[2*], Alpaslan Demirci[3], Erdin Gökalp[4]

[1]Yıldız Technical University, Faculty of Electrical and Electronics Engineering, Department of Electrical Engineering, Istanbul, Türkiye.
*[2]Yıldız Technical University, Faculty of Electrical and Electronics Engineering, Department of Electrical Engineering, Istanbul, Türkiye.
[3]Yıldız Technical University, Faculty of Electrical and Electronics Engineering, Department of Electrical Engineering, Istanbul, Türkiye.
[4]Yıldız Technical University, Faculty of Electrical and Electronics Engineering, Department of Electrical Engineering, Istanbul, Türkiye.
[1]ORCID Code: -
*[2]ORCID Code: **0000-0002-4411-411X**
[3]ORCID Code: **0000-0002-1038-7224**
[4]ORCID Code: **0000-0002-1518-432X**
* musa.terkes@yildiz.edu.tr

ABSTRACT

The rapid integration of renewable generation, distributed resources, and electric vehicle (EV) charging infrastructure has imposed new challenges on the design and operation of modern industrial power systems. In this study, a comprehensive framework is developed for the medium-voltage/low-voltage (MV/LV) distribution transformer substation of a large-scale industrial facility, where conventional production-related electrical demands are combined with 33 units of 22 kW EV charging stations. The methodology encompasses detailed design calculations including cable sizing and voltage drop analysis, busbar dimensioning, transformer selection, compensation panel design with step calculation, and short-circuit analysis in accordance with IEC standards, covering both symmetrical and asymmetrical conditions as well as thermal and dynamic withstand currents. Additional considerations such as fault current contributions from DC components, specification of circuit breakers, and the selection of measurement and metering devices are incorporated to ensure robustness and compliance. The final design is validated through load flow and short-circuit simulations conducted in ETAP, confirming technical consistency and operational feasibility. Beyond addressing individual technical aspects, the proposed approach provides an integrated solution that bridges traditional industrial power system design with the emerging requirements of EV infrastructure. This contribution enhances system efficiency, reliability, and adaptability, and offers a practical reference for the future planning of industrial facilities in an evolving energy landscape.

Keywords: Industrial power systems, MV/LV distribution transformer substation, electric vehicle charging infrastructure, cable sizing and voltage drop analysis, power system reliability and efficiency, load flow analysis, short-circuit analysis, grid integration.

INTRODUCTION

The rapid evolution of industrial facilities and the integration of renewable and distributed energy resources have significantly reshaped the design and operation of modern power distribution systems. Recent studies highlight the increasing complexity of load forecasting, optimization, and system integration in environments where multiple consumption and generation patterns coexist, requiring advanced methodologies to ensure efficiency, stability, and sustainability (Esmaeeli et al., 2015). Hybrid modeling approaches combining data-driven techniques with domain-specific engineering insights have been widely adopted to capture nonlinear dynamics, uncertainty, and operational variability across diverse contexts (Yosef, Sayed and Youssef, 2015). Moreover, advances in interpretability and uncertainty quantification have demonstrated the importance of reliable decision-making in the design of resilient energy infrastructures (Ziari, Ledwich and Ghosh, 2011).

The integration of electric vehicle (EV) charging infrastructure into industrial and commercial facilities adds another layer of technical and operational challenges. Researchers have addressed multi-stage optimization strategies that simultaneously minimize costs and preserve battery health, highlighting the dual objective of economic efficiency and system longevity (González-Sotres et al., 2013). Additionally, hybrid artificial intelligence (AI) forecasting frameworks that combine temporal modeling with ensemble strategies have been successfully applied to both energy demand and generation, underscoring their potential to inform infrastructure planning and grid operation (Rupolo et al., 2017). These approaches are further strengthened by multitask learning and deep neural architectures, which capture temporal dependencies while preserving explainability (Deakin et al., 2021). Such methodologies enable a more comprehensive treatment of time-series behaviors and provide critical insights for robust electrical system design (Rodriguez-Calvo et al., 2014).

Parallel to methodological advancements, practical applications in distribution system planning have incorporated uncertainty analysis and interpretability, ensuring that models not only achieve accuracy but also deliver trustworthy recommendations (Mendoza et al., 2012). For industrial loads, the necessity of accounting for diverse profiles, including renewable generation, storage, and mobility electrification, has been emphasized in recent studies (Haghifam et al., 2015). Moreover, ensemble frameworks combining machine learning models with optimization techniques have proven particularly effective in energy market forecasting and operational scheduling, reinforcing their applicability to infrastructure planning (Sikora et al., 2024). Recent contributions also underline the relevance of explainable AI in energy systems, offering stakeholders transparent justifications for model-driven design and operational choices (Jabbar et al., 2025).

The literature further demonstrates the need for generalizable frameworks that remain effective across varying temporal, spatial, and contextual conditions (Pisano et al., 2023). This adaptability is crucial when extending design principles to industrial facilities, where the simultaneous presence of high-demand manufacturing processes and EV charging infrastructure creates substantial planning challenges (Mancini et al., 2020). Uncertainty estimation techniques, such as Monte Carlo (MC) dropout, complement these approaches by providing risk-aware insights into future demand scenarios, thereby enhancing system robustness (Marah et al., 2016). In addition, optimization-driven ensemble models have highlighted the importance of balancing accuracy, interpretability, and computational efficiency, offering pathways to scalable and practical solutions for real-world infrastructures (Mogos and Grillo, 2021).

Against this backdrop, the present study addresses the comprehensive design of an MV/LV distribution transformer substation for a glass factory, incorporating both industrial electrical demands and 33 units of 22 kW EV charging stations. The proposed work delivers a holistic framework that includes cable sizing and voltage drop analysis, busbar design, transformer selection, compensation panel dimensioning, short-circuit calculations in compliance with IEC standards, fault current withstand capability assessment, protective device specification, and metering equipment selection. The design is validated through load flow and short-circuit simulations in ETAP, ensuring technical consistency and operational feasibility. This contribution is not only necessary but also original, as it integrates conventional industrial power system design with the emerging requirements of EV infrastructure, providing a comprehensive solution that enhances efficiency, reliability, and adaptability in modern industrial facilities.

COMPREHENSIVE DESIGN FRAMEWORK AND EQUIPMENT SELECTION

System Description

The power distribution system of the facility under consideration is supplied from the national transmission grid at 154 kV, which is initially stepped down to 11 kV through transformer TR-B and then distributed to the medium-voltage (MV) busbar via the TR-D substation at 6.3 kV. From this point, the industrial processes are supplied through existing feeders, while the proposed design introduces an additional substation to meet both the conventional production-related demands and the newly planned EV charging infrastructure. The new substation includes a 2.5 MVA, 6.3/0.4 kV transformer (TR-2), directly connected to the MV busbar, which supplies nine independent low-voltage (LV) distribution panels through aluminum busbars and dedicated feeders. The technical characteristics of the transformers are summarized in Table 1. To ensure technical compliance and operational reliability, detailed calculations were carried out during the design process. These include cable sizing and voltage drop verification, busbar dimensioning, transformer selection, compensation panel design with step sizing, and short-circuit calculations in accordance with IEC standards, covering both symmetrical and asymmetrical fault conditions. The design also incorporates the evaluation of thermal and dynamic withstand currents, contributions from DC fault components, as well as the specification of circuit breakers, protection devices, and metering equipment. Table 1 and Figure 1 provide a general overview of the system.

The main loads connected to the planned LV switchboard are listed in Table 2, together with their power ratings, distances, and power factors. In line with the operator's technical requirements, the system power factor is targeted to be improved to approximately 0.99 by means of a staged compensation system, designed to follow the dynamic load variations. Furthermore, cost optimization was considered a primary objective by the operator; therefore, circuit breaker and cable selections were restricted to specific series and models provided by a single manufacturer, ensuring a balance between technical adequacy and economic feasibility.

Table 1. Transformer Information in the Project

Transformer	Rated Power (MVA)	Turn Ratio	Winding Connection (Vector Group)	$\%u_k$
TR-B	50	154 kV /11 kV	YNd1	17
TR-D	25	11 kV / 6.3 kV	Dyn11	10
TR-2 (planned)	To be determined	6.3 kV / 0.4 kV	To be determined	To be determined

Table 2. Loads Included in the Project

Feeder No.	Load	Active Power (kW)	Distance (m)	cos φ
F01	F2-MDP-8	280	140	0.85
F02	UT-COMP7-3	292	100	0.82
F03	UT-COMP7-4	292	100	0.82
F04	F2-MZ-DP	165.6	140	0.87
F05	HOT-20	195.16	140	0.82
F06	F2-UO-DP	214.63	100	0.89
F07	UT-MCC.CT	72	130	0.90
F08	F2-MCC.1	190.2	100	0.85
F09	UT-MDP	596.91	40	0.87
F10	EV charging station panel	726	300	0.82

Design and Selection

- MV/LV Transformer Sizing

The selection of transformers is a fundamental engineering step to ensure the stability, safety, and efficiency of power distribution systems. This process is not only determined by the connected load but also by several technical

parameters, including the system power factor, demand factor, short-circuit characteristics, winding connection group, harmonic effects, and economic losses.

The transformer rating can be determined by considering the installed load (P_k, 3024.5 kW), demand factor (T_f, 0.8), cos φ power factor of the system (0.99), and system losses (k_f, 1.1 or 10% loss) as follows:

$$S_{Tr} = \frac{P_k . k_f . T_f}{\cos \varphi} \tag{1}$$

As a result, the transformer capacity is selected as the nearest higher standard rating, 3150 kVA, in compliance with IEC 60076. The main technical specifications of the selected transformer are summarized as follows:

- **Rated Power:** 3150 kVA
- **Primary/Secondary Voltage:** 6.3 kV / 0.4 kV
- **Short-Circuit Impedance (%u_k):** 6%
- **Winding Connection (Vector Group):** Dyn11
  - The low-voltage winding is star-connected (Y), while the high-voltage winding is delta-connected (D). The group index "11" indicates a 30° phase displacement between the HV and LV sides.
- **Frequency:** 50 Hz
- **Cooling Type:** ONAN

The selection of Dyn11 connection provides a neutral point on the LV side, ensures proper operation under unbalanced load conditions, and offers favorable harmonic performance. In addition, the short-circuit impedance of 6% supports adequate fault current limitation and facilitates reliable protection coordination.

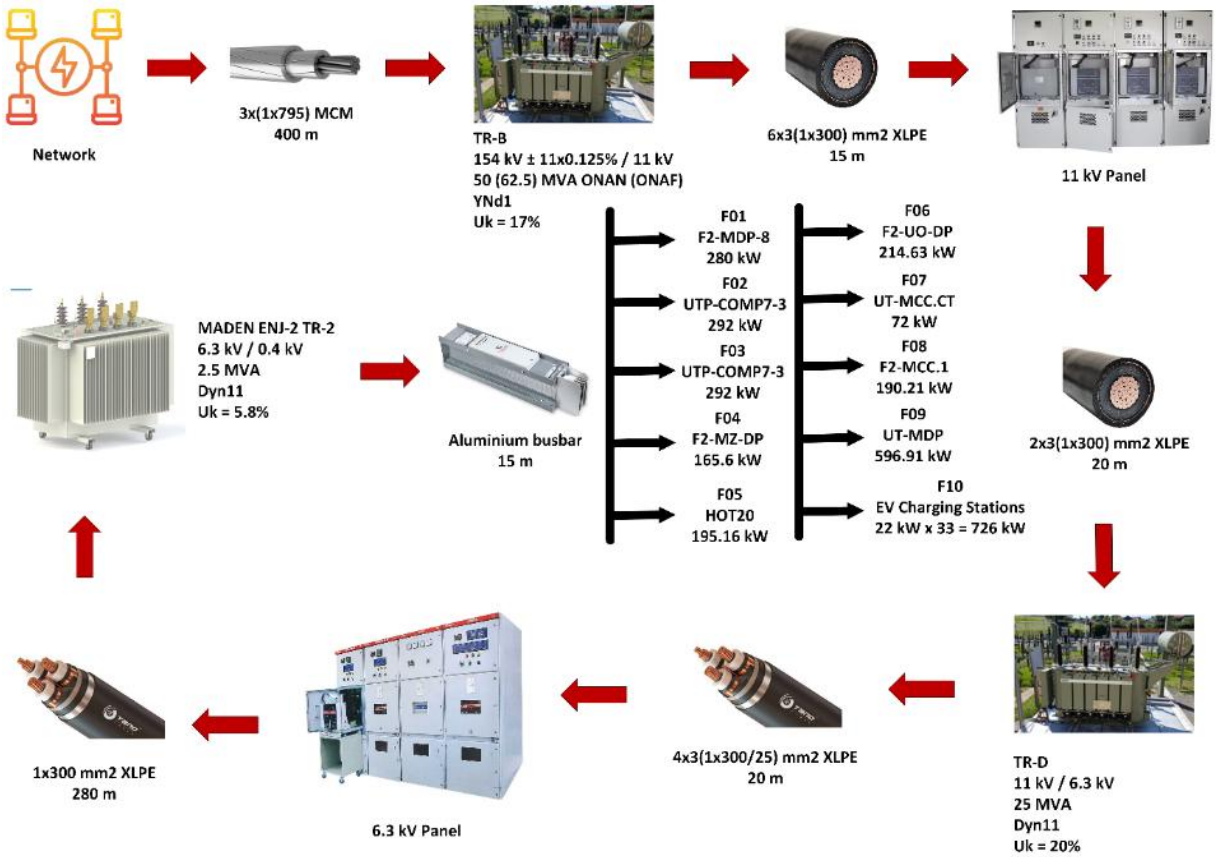


Figure 1. Designed Project

- Compensation System

Reactive power compensation plays a vital role in maintaining the power factor at the desired level, improving energy efficiency, and minimizing losses in industrial facilities. In addition to enhancing energy quality, compensation systems help to prevent penalties imposed by utilities for low power factor operation.
The required compensation power was determined by considering the difference between the existing and the targeted power factor, as expressed in Equation (2):

$$Q = P_k.k \quad or \quad Q = P_k.(\tan\varphi_1 - \tan\varphi_2) \quad ; \\ \varphi_1 : available, 0.8\ power\ factor \ ; \ \varphi_2 : desired, 0.99\ power\ factor \tag{2}$$

Thus, the total required compensation was calculated as 1693.72 kVAr. A portion of the required reactive power was allocated to fixed compensation to cover the transformer's base load. According to IEC recommendations, this value is typically selected between 3–5% of the transformer's rated power. Therefore, the fixed compensation value is 125 kVAr. The remaining portion was distributed to an automatic stepwise capacitor bank controlled by a reactive power relay (1568.72 kVAr). A 12-step compensation relay was selected, and the capacitor sizes per step were defined to provide flexible adjustment to the varying load profile. The distribution of capacitor ratings is presented in Table 3.

Table 3. Compensation Stages

Stage	Reactive Power (kVAr)	Stage	Reactive Power (kVAr)	Stage	Reactive Power (kVAr)
Fixed	125	Stage 4	100	Stage 8	150
Stage 1	20	Stage 5	100	Stage 9	150
Stage 2	50	Stage 6	150	Stage 10	200
Stage 3	100	Stage 7	150	Stage 11-12	200 & 200

- Cable Sizing and Selection Criteria

Cable sectioning and voltage-drop verification were performed in accordance with IEC 60364-5-52. The procedure follows a standard engineering workflow: **(i)** determine the required load current from active power and power factor, **(ii)** select a candidate cable section from manufacturer tables, **(iii)** apply installation and grouping correction factors to obtain the corrected ampacity, **(iv)** verify that corrected ampacity ≥ required current, and **(v)** evaluate voltage drop for the chosen conductor and confirm %ΔV is within allowable limits (IEC guidance for LV distribution: typically ≤ 3–5% depending on local practice; here the design target is ≤ 5%).
Therefore, three-phase load current is calculated by:

$$I = \frac{P}{\sqrt{3}.U.\cos\varphi} \tag{1}$$

where I load current [A], P active power [W], U line voltage [V] (400 V used here), and $\cos\varphi$ power factor. All feeder currents reported below are computed by Equation (3) and rounded to two decimals.
The cable ampacity used for verification is the manufacturer's nominal ampacity modified by correction factors that account for installation method, grouping and ambient conditions: **(i)** correction factor k_d depends on routing (in air, in conduit, buried), number of systems, ambient temperature and ventilation. The project used the correction factors from the manufacturer/IEC tables as provided in the design documents (examples in the table below). **(ii)** corrected ampacity = (nominal ampacity) × k_d × (number of parallel systems when applicable). The design assumed the installation conditions you specified (well-ventilated cable trays for most feeders, some buried runs for EV feeder), and used the k_d values you provided. Overall, selected cable sections and ampacity checks present in Table 4. (**Note:** PFC power factor correction.)

Table 4. Cable Cross-sections and Current Carrying Capacity Checks

Feeder / Panel	P (kW)	cos φ	I (A)	Installation	Systems	k_d	Selected Cable	Corrected Ampacity (A)	Check
F2-MDP-8	280	0.85	475.46	Vent. tray	2	0.97	2×(3×1×95 mm²) XLPE	> 475.46	**OK**
UT-COMP7-3	292	0.82	513.98	Vent. tray	2	0.94	2×(3×1×70 mm²) XLPE	658	> 513.98 → **OK**
UT-COMP7-4	292	0.82	513.98	Vent. tray	2	0.94	2×(3×1×70 mm²) XLPE	658	**OK**
F2-MZ-DP	165.6	0.87	274.74	Vent. tray	2	0.97	2×(3×1×50 mm²) XLPE	> 274.74	**OK**
HOT-20	195.16	0.82	343.52	Vent. tray	2	0.97	2×(3×1×70 mm²) XLPE	> 343.52	**OK**
F2-UO-DP	214.63	0.89	348.08	Vent. tray	1	1.00	3×1×70 mm² XLPE	> 348.08	**OK**
UT-MCC.CT	72	0.90	115.47	Vent. tray	1	1.00	3×35 mm² XLPE	> 115.47	**OK**
F2-MCC.1	190.21	0.85	322.99	Vent. tray	1	1.00	1×95 mm² XLPE	> 322.99	**OK**
UT-MDP	596.91	0.87	990.31	Vent. tray	3	0.96	3×(3×1×95 mm²) XLPE	1008	> 990.31 → **OK**
EV charger panel	726	0.82	1277.92	Buried	5	0.70	5×(3×1×240 mm²) XLPE	2730	> 1277.92 → **OK**
EV charger (unit)	22	0.82	38.72	Buried	1	1.00	3×4 mm² XLPE	~52 (corrected)	52 > 38.72 → **OK**
PFC panel	- 1695 kVAr	-	2446.52	Vent. tray	4	0.94	4×(1×240 mm²) XLPE	2932.8	**OK**

- Busbar Sizing and Selection Criteria

Busbar sizing follows the same principles as cable sizing but relies on rectangular or tubular busbar catalogue data, including manufacturer-provided resistance and reactance per unit length, mechanical ratings, and current capacity. The following sequence is considered for each busbar run:

1. Computes the design current I from the supplying source (transformer or panel) using Equation (3) or from the sum of the outgoing feeder currents.
2. Selects a busbar with a rated current higher than the design current, applying an engineering margin to account for mechanical and thermal considerations. For compensation busbars, they typically apply an additional margin of +20% to accommodate switching inrush and transient conditions.
3. Confirms that the chosen busbar profile satisfies mechanical strength, short-time current withstand, and temperature rise requirements. The busbar selections are based on manufacturer catalogue values and provide the required ampacity plus mechanical and thermal margins. The busbar features selected according to the relevant criteria are explained in Table 5.

Table 5. Selected Busbars

Busbar location	Nominal current (A)	Selected cross-section	Manufacturer rated capacity (A)	R (mΩ/m)	X (mΩ/m)
Transformer → ADP (TR-2 to TR-DP-2.1)	4409.59	3 × (6 × 180) mm rectangular alu	5000	0.017	0.008
Compensation busbar	2444.67 (design) → use 1.2 margin → 2933.61	2 × (6 × 180) mm rectangular alu	3300	0.017	0.01
EV charger station busbar	1277.92	6 × 160 mm rectangular alu	1600	0.081	0.019

- Voltage-drop Calculation

Voltage drop was calculated using the standard three-phase formula:

$$\Delta V = \sqrt{3}.I.L.(R'\cos\varphi + X'\sin\varphi) \quad (4)$$

where ΔV voltage drop [V], one-way conductor length [m], R' series resistance per unit length [Ω/m] (for the selected conductor), X' series reactance per unit length [Ω/m], and $\cos\varphi$, $\sin\varphi$ load power factor components. Percentage voltage drop is:

$$\%e = \frac{u}{U_0}100 \quad (5)$$

where U_0 is phase-to-neutral nominal voltage (≈230 V) when reporting phase-to-neutral percentage or use $U = 400\ V$ for phase-to-phase percentage depending on reporting convention. The analysis is conducted on a phase-to-neutral basis, where appropriate, to ensure consistency with the project tables.

For cable calculations, per-meter resistance R' is obtained from conductor resistivity data: $R' = \rho/S$ (where ρ is the conductor resistivity in Ω·mm²/m and S the cross-section in mm²). Typical values used in the design: copper $\rho \approx 0.0225$ Ω·mm²/m (conservative table value), and the per-unit reactance λ taken as 0.08 mΩ/m (0.00008 Ω/m) unless manufacturer data specify otherwise. (**Note:** Apart from the subject, R' and X' for busbars are taken directly from the busbar catalogue.)

All cable voltage-drop computations were performed with Equation (4) and results summarized below. The acceptance criterion is $\Delta V \leq 5\%$. All computed cable % voltage drops are below the design limit of 5% in Table 6. The EV charging panel run is close to the upper limit (4.95%); that routing and conductor sizing were therefore checked in ETAP as part of the final verification.

The voltage drop on busbars is evaluated using two complementary approaches. The first approach follows the classical voltage drop expression (Equation 6), while the second considers both the ohmic resistance and the reactance of the busbar (Equation 7).

$$\%e = \frac{100.P.L}{\kappa.S.U^2} \quad (6)$$

where P power [W], L length [m], κ conductivity coefficient [m/Ω·mm²], S conductor cross-section [mm²], and U line-to-line voltage [V].

$$\%e = \frac{\sqrt{3}.I_b.L.(R_{bus}\cos\varphi + X_{bus}\sin\varphi)}{U}100 \quad (7)$$

where I_b design current [A], R_{bus} ohmic resistance [mΩ/m], X_{bus} reactance [mΩ/m], φ load power factor angle, and L length [km]. Table 7 describes the busbar voltage drop controls. All busbar sections satisfy the IEC 60364-5-52 voltage drop criterion (<5%).

- Short-Circuit Calculations and Equipment Selections

Short-circuit analyses were performed to determine the maximum (sub-transient), instantaneous (peak) and thermal (1 s) fault currents at critical points of the distribution system, and to verify the adequacy of circuit-breakers and instrument transformers. Calculations follow IEC 60909 and use the per-unit (pu) modelling approach with a 100 MVA common base.

a. Per-unit base: $S_{base} = 100\ MVA$. Base voltages used at each voltage level correspond to the actual system (154 kV, 11 kV, 6.3 kV, 0.4 kV) and scaling is performed accordingly.

b. Voltage tolerance ("c" factor): maximum fault calculations use $c_{max} = 1.05$; minimum (relay pick-up / minimum-fault) calculations use $c_{min} = 0.95$. This accounts for pre-fault voltage excursions per IEC 60909.

c. Transformer data: nameplate %uk and vector group information (e.g. TR-B: 50 MVA, %uk=17, YNd1; TR-D: 25 MVA, $\%u_k$ = 10, Dyn11; TR-2: 3.15 MVA, $\%u_k \approx 5.8$, Dyn11) were used. Transformer resistive

component (u_{Rr}) was included where available and transformer correction factor K_T was applied to represent real operating characteristics.

d. Line and cable impedances: R and X per unit-length were taken from the referenced manufacturer / standard tables. For minimum-current evaluations (relay pick-up), conductor resistances were corrected to 70 °C using the standard temperature correction factor $(1/(1 + 0.0039.\Delta T))$.

Table 6. Cable Voltage Drops Results

Feeder / Panel	I (A)	Distance (m)	Conductor	Systems	Section (mm²)	ΔV (V)	$\%\Delta V$	Status
F2-MDP-8	475.46	140	Cu	2	95	8.56	3.7	**OK**
UT-COMP7-3	513.98	100		2	70	8.76	3.79	**OK**
UT-COMP7-4	513.98	100		2	70	8.76	3.79	**OK**
F2-MZ-DP	274.74	140		2	50	9	3.9	**OK**
HOT-20	343.52	140		2	70	8.19	3.55	**OK**
F2-UO-DP	348.08	100		1	70	8.17	3.54	**OK**
UT-MCC.CT	115.47	130		1	35	9.72	4.21	**OK**
F2-MCC.1	322.99	100		1	95	7.94	3.44	**OK**
UT-MDP	990.31	40		3	95	3.54	1.53	**OK**
EV charger panel	1277.92	300		5	240	11.44	4.95	**OK** (border line)
EV charger (unit)	38.72	10		1	4	-	-	**OK**
PFC panel	2446.52	30		4	240	4	1.1	**OK**

Table 7. Calculated Busbar Voltage Drops

Busbar Section	Length (m)	Current (A)	Cross-section	% Voltage Drop	Compliance
Transformer – Main Dist. Panel	15	4409.6	3 × (6 × 180)	0.553	<5% **(✓)**
Compensation panel	2	2444.7	2 × (6 × 180)	0.07	
EV charger station	5	1277.9	6 × 160	0.21	

e. R/X dependent peak factor: the peak (first-peak) multiplier κ was computed using the project's adopted expression:

$$\kappa = 1.02 + 0.9.e^{-\frac{3R}{X}} \tag{8}$$

where $\frac{R}{X}$ is the equivalent resistance/reactance ratio of the network seen from the fault location.

Thermal and mechanical checks: the thermal withstand current I_{th} (1 s) was computed using the project's adopted interaction of DC and AC heating components (m and n coefficients obtained from IEC/figure-based curves). Where graphical m or n data were required, the same reference charts used in the project were applied.

The table below reproduces the per-unit impedances used in the project after conversion to the 100 MVA base.

These per-unit numbers were summed and reduced to the fault level with standard voltage-ratio reduction factors (D) per IEC 60909. Reduction to the fault level and the intermediate reduced-impedance tables are given in Table 9 and 10 of the project. The following sequence was applied for each fault location:

Reduce all equipment impedances to the fault voltage level using the appropriate transformation ratios / reduction factors (D) per IEC 60909. This yields the total reduced positive-, negative- and zero-sequence impedances seen from the fault point.

Compute the equivalent fault impedance Z_k (ohmic value at the fault voltage level) from the reduced per-unit values. Then, calculate the sub-transient (symmetrical) three-phase current using the maximum voltage factor c_{max}:

$$I_{k3} = \frac{c_{max} U_{LL}}{\sqrt{3}. Z_k} \tag{9}$$

Table 8. Selected Element Impedances on 100 MVA Base (pu)

Element	Voltage (kV)	$R_{1\text{-}2}$ (pu)	R_0 (pu)	$X_{1\text{-}2}$ (pu)	X_0 (pu)
Transmission system (infeed)	154	0.00119	0.00119	0.0119	0.0238
TR-B (154/11)	154/11	0	0	0.34	0.34
TR-D (11/6.3)	11/6.3	0	0	0.4	0.4
TR-2 (6.3/0.4)	6.3/0.4	0	0	1.8412	1.8412
3×(1×795) MCM (OH line)	154	0.000139	0.000392	0.000544	0.00158
6×3×(1×300) XLPE	11	0.000777	0.006995	0.000312	0.00156
2×3×(1×300) XLPE	11	0.00104	0.00933	0.000415	0.00208
4×3×(1×300) XLPE	6.3	0.00316	0.0316	0.00127	0.0114
3×(1×300) XLPE	6.3	0.0442	0.442	0.0177	0.1596

Subsequently, compute the peak (first-peak) current:

$$I_p = \sqrt{2}. \kappa. I_{k3} \tag{10}$$

After, compute thermal (1 s) withstand current I_{th} using the project's methodology (m and n coefficients extracted from the referenced figures for the chosen κ and clearing time T_k):

$$I_{th} \approx I_{k3}. \sqrt{m + n} \tag{11}$$

Exact m and n were taken from the standard charts used in the project; the values used appear in the results table. Minimum (relay-pickup) currents and single-phase-to-earth calculations were computed using the minimum voltage factor c_{min} and conductor resistances at 70 °C (as per IEC tables) to ensure that protection relays see reliably detectable current.

All numerical results below follow the project's reduction steps and the formulas above. Results are presented for the two critical fault locations that were analyzed in detail.

Table 9. Symmetric and Asymmetrical Short-Circuit Results (Selected Fault Points)

Fault point (bus)	Voltage level	Z_k (Ω)	$I_{k3}(kA)$	κ	$I_p(kA)$	$I_{th}(1\ s)(kA)$
Point 1 — TR-2 primary (6.3 kV bus)	6.3 kV	0.3221	11.86	1.804	30.03	12.13
Point 2 — TR-2 secondary (0.4 kV bus)	0.4 kV	0.00422	57.46	1.786	145.15	58.56

Notes on table entries: I_{k3} is the sub-transient (symmetrical) three-phase fault current computed with $c_{max} = 1.05$ and a clearing time $T_k = 0.5 - 1.0\ s$ as used in the project.

The minimum single-phase-to-earth calculation at the TR-2 secondary gives a worst-case single-phase current of approximately 49.12 kA (project calculation). This value was used to confirm relay operating margins and minimum pickup adequacy.

Thermal (1 s) currents I_{th} for the two evaluated locations were found to be 12.13 kA (Point 1) and 58.56 kA (Point 2). Conductors and busbars were checked against these values for short-time thermal capability and the mechanical (electrodynamic) effects of the peak current I_p. All selected conductor/busbar cross-sections were confirmed to withstand the computed thermal energy (I^2t) and the dynamic forces based on the project's verification tables.

- Circuit-breaker Selection

Circuit-breaker selections were made to satisfy the peak, symmetric and thermal requirements derived above; additionally rated continuous currents were checked against steady-state load currents.

a. Breaking capacity (1 s short-time or rated ultimate breaking capacity) > computed I_{k3} and with adequate margin for test/standard ratings.

b. Peak withstand (I_{cm} or I_{ma}) ≥ computed I_p or mechanical withstand requirement.

c. Rated continuous current I_n ≥ steady state operating current with margin for foreseeable load growth.

d. Standards compliance: IEC 62271-100 for MV breakers, IEC 60947-2 for LV breakers.

The breaker selections and series were chosen to balance technical adequacy and the operator's cost restriction (allowed vendor/series). All selected breakers exceed the calculated sub-transient and peak currents with appropriate safety margin (see Table 10).

Table 10. Selected Main Circuit-breakers

Location / Function	Device (project selection)	Key ratings (project)	Rationale
6.3 kV main (TR-D → TR-2 primary)	Siemens SION 3AE5 (VCB)	I_n **:** 800 A I_{sc} **(1 s):** 16 kA I_{ma} **:** 40 kA	VCB selected for MV line, breaking capacity > computed $I_{k3} = 11.86$ kA; peak withstand sufficient ($I_{ma} = 40$ kA).
0.4 kV main (TR-2 secondary)	Siemens 3WL1350 (ACB)	I_n **:** 5000 A I_{sc} **(1 s):** 100 kA I_{cm} **:** 220 kA	ACB selected for LV main: rated continuous current (5 kA) > steady source current (4.546 kA) and short-circuit/peak ratings well above computed 57.46 kA sub-transient and 145.15 kA peak.
Distribution feeders	MCCB / ACB per feeder (Siemens 3VA2 / 3WA11, etc.)	See **Table 11**.	Selections match each feeder's steady current and short-circuit requirements (MCCB for lower-current feeders; ACB for high-demand feeders).

Table 11. Selected Circuit Breakers for Load Feeders

Load No	Load Name	Power [kW]	Rated Current [A]	Selected Product	Selected Circuit Breaker [A]
F01	F2-MDP-8	280	475.46	MCCB series	Siemens 3VA2
F02	UT-COMP7-3	292	513.98	4 × 630	Siemens 3VA2 4 × 800
F03	UT-COMP7-4	292	513.98	MCCB series	Siemens 3VA2
F04	F2-MZ-DP	165.6	273.89	4 × 800	Siemens 3VA2 4 × 400
F05	HOT-20	195.16	343.52	MCCB series	Siemens 3VA2
F06	F2-UO-DP	214.63	346.89	4 × 630	Siemens 3VA2 4 × 630
F07	UT-MCC.CT	72	115.94	MCCB series	Siemens 3VA2
F08	F2-MCC.1	190.2	324.30	4 × 250	Siemens 3VA2 4 × 630
F09	UT-MDP	596.91	988.39	ACB	Siemens 3WA11 4 × 1250
F10	EV charging station	726	1277.92	ACB	Siemens 3WA11
-	EV chargers	22	38.72	4 × 1600	Siemens 3VA2 4 × 63
-	PFC panel	1695 kVAR	2446.52	ACB	Siemens 3WA12 4 × 3200

- Instrument Transformer Selection (CTs and VTs)

TR-2 primary (6.3 kV side): system nominal primary ≈ 288.7 A → current transformer (CT) selected as 300/5 A, burden ≈ 15 VA, dual accuracy: 0.5 (measurement) and 5P20 (protection). The CT thermal withstand was verified against the computed thermal short-circuit current at that point (≥ 12.13 kA, 1 s).

TR-2 secondary (0.4 kV side): system nominal primary ≈ 4 546.6 A → CT chosen as 5000/5 A, burden ≈ 20 VA, accuracy classes: 0.5 (measurement) / 5P20 (protection). CT's specified short-time thermal and accuracy characteristics were selected to tolerate the highest calculated fault currents (sub-transient and thermal values: 57.46 kA and 58.56 kA respectively).
Operational remarks: CT burden (VA) sizing included the combined connected devices (meters, relays, recorders) and cable lead losses (5 m secondary runs as in the project). Dual-class CTs (measurement + protection) were specified in order to support both energy/quality metering and high-speed protective relays.
Voltage transformers (VTs) for protection and metering at the TR-2 primary were specified as 6.3/0.1 kV, 20 VA, class 0.3 (measurement) and class 3 (protection) to provide the required accurate voltage signals for directional relays and metering functions.
The IEC 60909-based short-circuit assessment and the per-unit modelling show that the chosen transformer ratings, conductor/busbar cross-sections and the selected protection and instrument transformer equipment meet the project's safety, thermal and electrodynamic requirements. In particular, the LV and MV main circuit-breakers provide sufficient continuous current rating, short-circuit breaking capacity and peak withstand capability relative to the computed sub-transient, peak and thermal currents. All computed results were verified against ETAP simulations.

SIMULATION-DRIVEN PERFORMANCE ASSESSMENT IN ETAP

ETAP-based load flow and short-circuit simulations demonstrate that the proposed electrical design operates reliably under both normal operating conditions and fault scenarios (see Figures 2-3). The load flow analyses show that voltage levels at all MV and LV busbars remain within ±5% limits. This confirms that the system operates stably under normal conditions, and that consumer voltage quality complies with relevant standards. The 1.583 MVAr capacity provided via the reactive power compensation panel effectively improves the power factor.
Cable and transformer loading levels, ranging between 60% and 95%, confirm that the equipment selection is appropriate. The TR-2 transformer operates at 91.4% on the primary side and 90.7% on the secondary side, representing the highest load levels in the system; however, these values remain within thermal limits. Busbar loadings are generally within acceptable levels. The only exception is the EV panel, which shows a 118.5% loading rate. However, this is a theoretical situation due to the EV charging infrastructure not being fully commissioned yet and does not pose a short-term practical risk. Furthermore, the total active losses are 131.6 kW, and reactive losses are 361.7 kVAr, indicating that losses remain within acceptable limits across the system.
In the short-circuit analysis, current values calculated for three-phase, two-phase, and single-phase-to-ground faults were verified through ETAP using the IEC 60909 method. The highest short-circuit current was recorded at the 0.4 kV TR-DP2.1 busbar, with 155.7 kA (three-phase) and 172.8 kA (single-phase-to-ground). These results highlight the significant influence of the zero-sequence impedance on asymmetric faults. At the MV level, a three-phase short-circuit current of 32.7 kA was calculated at the 6.3 kV MV panel 2 busbar, typical for MV systems and compliant with equipment withstand ratings. The simulation results confirm that circuit breakers meet continuous current capacity, short-circuit interrupting capacity, and thermal withstand requirements safely.
Time-domain analyses show that the system is exposed to its highest thermal and electrodynamic stresses during the initial cycles following the fault initiation. As seen in the ETAP outputs, the DC component decays rapidly within the first few hundred milliseconds, while the AC component exhibits oscillatory behavior during the initial cycles before stabilizing. This finding is critical for circuit breaker selection and protection coordination, reinforcing the importance of first-cycle withstand capability as emphasized by IEC 60909.
Additionally, ETAP outputs not included in the report indicate that peak inrush currents in LV panels align with the theoretical maximum values specified in the simulation report. These outputs also show that some heavily loaded cables approach more than 80% of their thermal limits during short-duration faults. While this does not present an immediate operational risk, it should be considered in future system expansion plans.
In conclusion, ETAP validations confirm that the proposed system design operates reliably, safely, and in compliance with standards under both normal conditions and various fault scenarios. Findings related to loading,

losses, short-circuit withstand levels, and protection coordination demonstrate that the equipment selections meet all technical requirements.

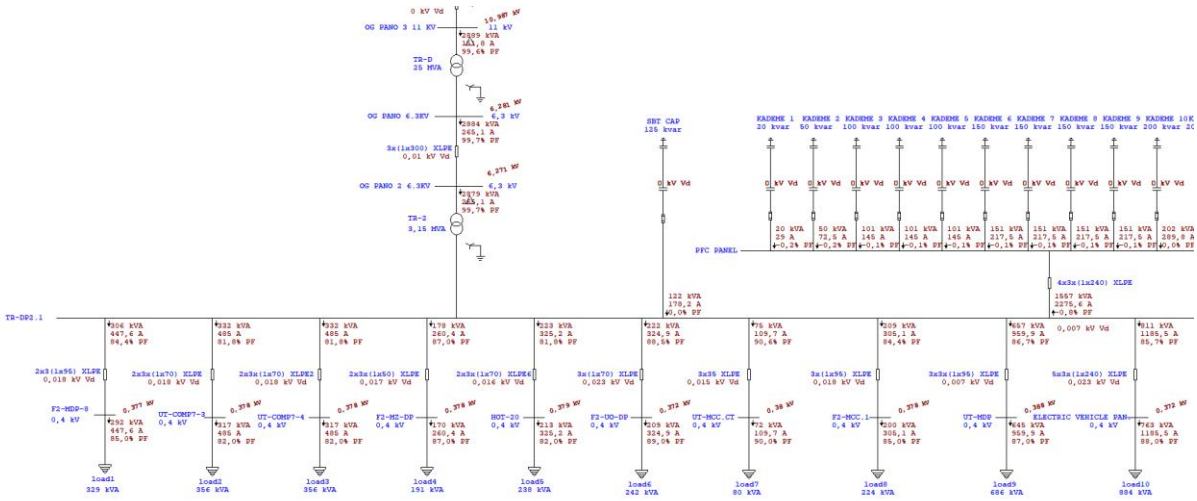


Figure 2. Load Flow Report

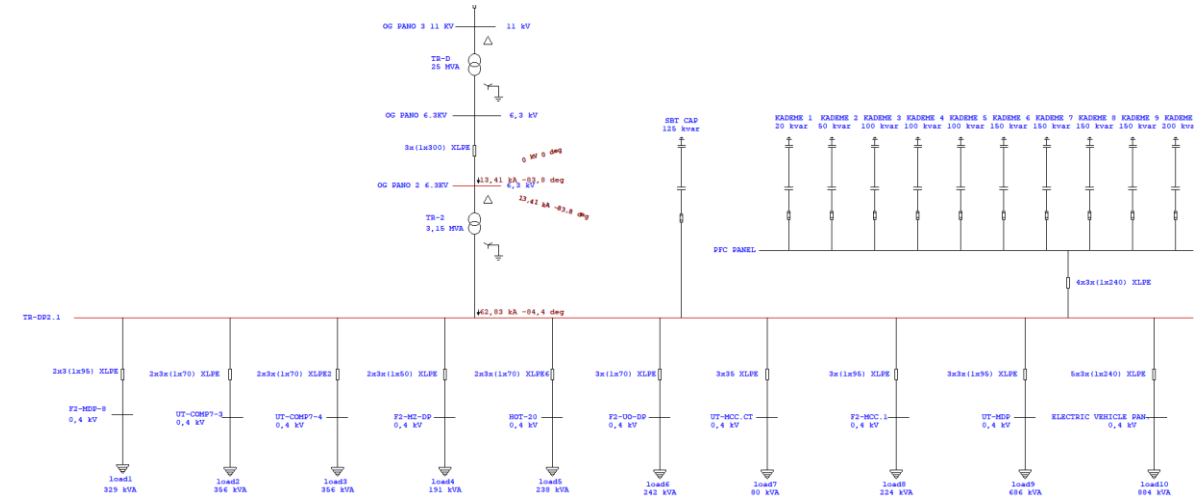


Figure 3. Short-Circuit Report

CONCLUSION AND FUTURE SUGGESTIONS

The study presented a comprehensive design and validation framework for an MV/LV distribution transformer substation that integrates both conventional industrial demands and an extensive EV charging infrastructure. By combining detailed analytical calculations with simulation-based assessments in ETAP, the proposed approach ensured that all components, from cable sizing and busbar dimensioning to transformer selection, compensation system design, and short-circuit withstand capability, comply with IEC standards and meet the operational requirements of the facility. The results demonstrated that the selected equipment operates within thermal and electrical limits, with load flows and voltage levels remaining stable under normal conditions and protection devices maintaining adequate margins under fault scenarios. Furthermore, the integration of staged reactive power

compensation improved the overall power factor to near unity, thereby enhancing efficiency and minimizing losses.

Beyond confirming the technical adequacy of the design, the findings underscore the significance of considering EV charging systems as integral rather than peripheral loads in industrial facilities. The high loading levels observed in the EV charging panel, although currently theoretical, highlight the necessity of anticipating future demand growth and planning for scalable infrastructure upgrades. Similarly, the short-circuit analyses emphasized the role of zero-sequence impedances in asymmetric faults, reinforcing the importance of robust protection coordination and first-cycle withstand capabilities.

Looking ahead, further research should explore the interaction between industrial loads and extensive EV charging demand, emphasizing advanced demand management and predictive optimization strategies. The integration of renewable generation, storage systems, and vehicle-to-grid technologies presents additional opportunities, with implications for transformer loading, fault behavior, and compensation design. Complementary techno-economic analyses that combine lifecycle cost, reliability, and sustainability perspectives would also strengthen decision-making. Overall, the proposed framework addresses immediate design requirements while providing a solid foundation for efficient, resilient, and adaptable power distribution systems in the evolving energy landscape.

REFERENCES

Deakin, M., Greenwood, D., Walker, S. and Taylor, P.C., 2021. Hybrid European MV–LV Network Models for Smart Distribution Network Modelling. In: *2021 IEEE Madrid PowerTech*. pp.1–6. https://doi.org/10.1109/PowerTech46648.2021.9494860.

Esmaeeli, M., Kazemi, A., Shayanfar, H.A. and Haghifam, M.-R., 2015. Multistage distribution substations planning considering reliability and growth of energy demand. *Energy*, [online] 84, pp.357–364. https://doi.org/https://doi.org/10.1016/j.energy.2015.03.002.

González-Sotres, L., Mateo Domingo, C., Sánchez-Miralles, Á. and Alvar Miró, M., 2013. Large-Scale MV/LV Transformer Substation Planning Considering Network Costs and Flexible Area Decomposition. *IEEE Transactions on Power Delivery*, 28(4), pp.2245–2253. https://doi.org/10.1109/TPWRD.2013.2258944.

Haghifam, M.-R., Esmaeeli, M., Kazemi, A. and Shayanfar, H., 2015. Optimal placement of the distribution substations to improve reliability under load growth. In: *2015 IEEE Power & Energy Society General Meeting*. pp.1–5. https://doi.org/10.1109/PESGM.2015.7286068.

Jabbar, A.A., Wanik, M.Z.C., Karaki, A. and Bayhan, S., 2025. Evaluating the Impact of Electric Vehicle Charging on MV/LV Distribution Network Using Distribution-Level Phasor Measurement Unit Data. In: *2025 IEEE 34th International Symposium on Industrial Electronics (ISIE)*. pp.1–6. https://doi.org/10.1109/ISIE62713.2025.11124655.

Mancini, E., Longo, M., Yaici, W. and Zaninelli, D., 2020. Assessment of the Impact of Electric Vehicles on the Design and Effectiveness of Electric Distribution Grid with Distributed Generation. *Applied Sciences*, [online] 10(15). https://doi.org/10.3390/app10155125.

Marah, B., Bhavanam, Y.R., Taylor, G.A. and Ekwue, A.O., 2016. Impact of electric vehicle charging systems on low voltage distribution networks. In: *2016 51st International Universities Power Engineering Conference (UPEC)*. pp.1–6. https://doi.org/10.1109/UPEC.2016.8114052.

Mendoza, J.E., López, M.E., Peña, H.E. and Labra, D.A., 2012. Low voltage distribution optimization: Site, quantity and size of distribution transformers. *Electric Power Systems Research*, [online] 91, pp.52–60. https://doi.org/https://doi.org/10.1016/j.epsr.2012.05.004.

Mogos, A.S. and Grillo, S., 2021. Impact of EV Charging Stations in Power Grids in Italy and its Mitigation Mechanisms. In: *2021 IEEE International Conference on Environment and Electrical Engineering and 2021 IEEE Industrial and Commercial Power Systems Europe (EEEIC / I&CPS Europe)*. pp.1–6. https://doi.org/10.1109/EEEIC/ICPSEurope51590.2021.9584782.

Pisano, G., Ruggeri, S., Soma, G.G., Falabretti, D., Grillo, S., Gulotta, F. and Pilo, F., 2023. Impact of Electrical Vehicle Private Charging Stations on the Quality of the Low Voltage Network Supply. *IEEE Open Access Journal of Power and Energy*, 10, pp.351–362. https://doi.org/10.1109/OAJPE.2023.3258254.

Rodriguez-Calvo, A., Frías, P., Reneses, J., Cossent, R. and Mateo, C., 2014. Optimal investment in smart MV/LV substations to improve continuity of supply. *International Journal of Electrical Power & Energy Systems*, [online] 62, pp.410–418. https://doi.org/https://doi.org/10.1016/j.ijepes.2014.04.062.

Rupolo, D., Pereira Jr, B.R., Contreras, J. and Mantovani, J.R.S., 2017. Medium- and low-voltage planning of radial electric power distribution systems considering reliability. *IET Generation, Transmission \& Distribution*, [online] 11(9), pp.2212–2221. https://doi.org/https://doi.org/10.1049/iet-gtd.2016.1478.

Sikora, R., Krajewski, Ł., Popenda, A. and Korzeniewska, E., 2024. Feasibility of Electric Vehicle Charging Stations from MV/LV Stations in Small Cities. *Energies*, [online] 17(24). https://doi.org/10.3390/en17246357.

Yosef, M., Sayed, M.M. and Youssef, H.K.M., 2015. Allocation and sizing of distribution transformers and feeders for optimal planning of MV/LV distribution networks using optimal integrated biogeography based optimization method. *Electric Power Systems Research*, [online] 128, pp.100–112. https://doi.org/https://doi.org/10.1016/j.epsr.2015.06.022.

Ziari, I., Ledwich, G. and Ghosh, A., 2011. Optimal integrated planning of MV–LV distribution systems using DPSO. *Electric Power Systems Research*, [online] 81(10), pp.1905–1914. https://doi.org/https://doi.org/10.1016/j.epsr.2011.05.015.